Applied Geochemistry 38 (2013) 33–47

Contents lists available at ScienceDirect

Applied Geochemistry

journal homepage: www.elsevier.com/locate/apgeochem

Metal release from dolomites at high partial-pressures of CO_2

Assaf Wunsch [a,b,*], Alexis K. Navarre-Sitchler [b,c], Joel Moore [d,e], Allison Ricko [d,e], John E. McCray [a,b]

[a] Civil and Environmental Engineering Department, Colorado School of Mines, 1500 Illinois St., Golden, CO 80401, USA
[b] Hydrologic Science and Engineering Program, Colorado School of Mines, 1500 Illinois St., Golden, CO 80401, USA
[c] Geology and Geological Engineering Department, Colorado School of Mines, 1500 Illinois St., Golden, CO 80401, USA
[d] Department of Physics, Astronomy and Geosciences, Towson University, 8000 York Road, Towson, MD 21252, USA
[e] Urban Environmental Biogeochemistry Laboratory, Towson University, 8000 York Road, Towson, MD 21252, USA

ARTICLE INFO

Article history:
Received 9 February 2013
Accepted 19 August 2013
Available online 27 August 2013
Editorial handling by M. Kersten

ABSTRACT

The potential for metal release associated with CO_2 leakage from underground storage formations into shallow aquifers is an important consideration in assessment of risk associated with CO_2 sequestration. Metal release can be driven by acidification of groundwaters caused by dissolution of CO_2 and subsequent dissociation of carbonic acid. Thus, acidity is considered one of the main drivers for water quality degradation when evaluating potential impacts of CO_2 leakage. Dissolution of carbonate minerals buffers the increased acidity. Thus, it is generally thought that carbonate aquifers will be less impacted by CO_2 leakage than non-carbonate aquifers due to their high buffering potential. However, dissolution of carbonate minerals can also release trace metals, often present as impurities in the carbonate crystal structure, into solution. The impact of the release of trace metals through this mechanism on water quality remains relatively unknown. In a previous study we demonstrated that calcite dissolution contributed more metal release into solution than sulfide dissolution or desorption when limestone samples were dissolved in elevated CO_2 conditions. The study presented in this paper expanded our work to dolomite formations and details a thorough investigation on the role of mineral composition and mechanisms on trace element release in the presence of CO_2. Detailed characterization of samples from dolomite formations demonstrated stronger associations of metal releases with dissolution of carbonate mineral phases relative to sulfide minerals or surface sorption sites. Aqueous concentrations of Sr^{2+}, CO^{2+}, Mn^{2+}, Ni^{2+}, Tl^{+}, and Zn^{2+} increased when these dolomite rocks were exposed to elevated concentrations of CO_2. The aqueous concentrations of these metals correlate to aqueous concentrations of Ca^{2+} throughout the experiments. All of the experimental evidence points to carbonate minerals as the dominant source of metals from these dolomite rocks to solution under experimental CO_2 leakage conditions. Aqueous concentrations of Ca^{2+} and Mg^{2+} predicted from numerical simulation of kinetic dolomite dissolution match those observed in the experiments when the surface area is three to five orders of magnitude lower than the surface area of the samples measured by gas adsorption.

1. Introduction

The dramatic increase in atmospheric concentrations of CO_2 over the last few centuries (IPCC, 2007) has led to mitigation efforts to reduce CO_2 emissions to the atmosphere. While ex situ options for sequestering CO_2 have been proposed (Bauer et al., 2011; Haug et al., 2010; Orlando et al., 2012; Perez-Lopez, 2008), the most promising mitigation technique, in terms of scale and storage potential, is geological carbon capture, utilization and storage (CCUS). Geological CCUS consists of injection of compressed CO_2 into deep saline geological formations or depleted oil and gas reservoirs. In the deep injection zone, supercritical CO_2 is less dense than formation waters resulting in buoyant upward movement of the CO_2. Structural trapping of CO_2 into the injection formation by overlying low-permeability caprocks should ensure containment. However, if leakage pathways exist in the caprock, such as improperly placed or sealed wells and faults or fractures, some CO_2 may migrate into shallower formations, leading to acidification of groundwater and potentially subsequent metal release from aquifer material through desorption and/or mineral dissolution. Where shallow aquifers are also underground sources of drinking water (USDWs), intrusion of CO_2 may lead to degradation of water quality (Carroll et al., 2009; Navarre-Sitchler et al., 2013; Siirila et al., 2012).

The effects of increased CO_2 concentrations on metal release in shallow aquifers have been studied using numerical simulation (Apps et al., 2010; Atchley et al., 2013; Navarre-Sitchler et al., 2013; Siirila et al., 2012; Wang and Jaffe, 2004; Wilkin and DiGiulio, 2010; Zheng et al., 2012), field studies (Kharaka et al., 2009;

* Corresponding author at: Civil and Environmental Engineering Department, Colorado School of Mines, 1500 Illinois St., Golden, CO 80401, USA. Tel.: +1 720 290 5133; fax: +1 303 273 3413.
E-mail address: assafwunsch@gmail.com (A. Wunsch).

0883-2927/$ - see front matter © 2013 Elsevier Ltd. All rights reserved.
http://dx.doi.org/10.1016/j.apgeochem.2013.08.005

Trautz et al., 2013) and laboratory experiments (Frye et al., 2012; Little and Jackson, 2010; Lu et al., 2010; Wei et al., 2011; Wunsch et al., submitted for publication). Harvey et al. (2013) provide a good review of results to date. In most studies, exposure of aquifer material to CO_2 increased aqueous concentrations of metals, though in one study, concentrations of several metals increased only temporarily (Lu et al., 2010). In another study concentrations of some metals decreased altogether (Little and Jackson, 2010).

In much of the current literature on potential impacts of CO_2 leakage on aquifers, the role of primary carbonate minerals (i.e., calcite and dolomite) is thought to be acting as a buffer to the increased acidity through carbonate mineral dissolution (Eqs. (1a) and (1b)) (e.g., Apps et al., 2010; Atchley et al., 2013; Wang and Jaffe, 2004):

$$CaCO_{3(Calcite)} + H^+ \rightleftharpoons Ca^{2+} + HCO_3^- \quad (1a)$$

and

$$CaMg(CO_3)_{2(Dolomite)} + 2H^+ \rightleftharpoons Ca^{2+} + Mg^{2+} + 2HCO_3^- \quad (1b)$$

It is also assumed in current literature that pH buffering from carbonate mineral dissolution will lower the risk of metal release into groundwater in aquifers where metals are sorbed to mineral surfaces or contained in oxides. As a result of this assumption, the risk of CO_2 leakage into carbonate aquifers has not been evaluated as extensively as non-carbonate aquifers. However, calcite and dolomite minerals often contain various minor and trace elements as impurities in solid-solution. Impurities such as Cd^{2+}, Fe^{2+}, Mg^{2+}, Mn^{2+}, Sr^{2+}, Co^{2+}, Zn^{2+}, Pb^{2+}, and Ba^{2+} may substitute for Ca^{2+} in the calcite lattice (Ahmed et al., 2008; Harstad and Stipp, 2007; Pingitore et al., 1992; Reeder et al., 1999). In addition, arsenate (AsO_4^{3-}), selenate (SeO_4^{2-}), sulfate (SO_4^{2-}) and chromate (CrO_4^{2-}) may substitute for CO_3^{2-} (Alexandratos et al., 2007; Aurelio et al., 2010; Bardelli et al., 2011; Reeder et al., 1994; Staudt et al., 1994; Tang et al., 2007). In dolomite minerals, cation substitution can occur either in the Ca^{2+} sites (Wright et al., 2002) or in the Mg^{2+} sites (Prissok and Lehmann, 1986). Adsorption of an impurity onto a carbonate mineral surface is considered a precursor to incorporation into the lattice in solid-solution (Ahmed et al., 2008; Comans and Middleburg, 1987). Therefore, the valence state of an impurity may affect the extent of substitution in the lattice, as evident for U (Sturchio et al., 1998) and As (Sø et al., 2008; Yokoyama et al., 2012). Given the presence of trace metal impurities in the carbonate mineral lattice, dissolution of primary carbonate minerals that provides buffering of pH can also result in co-release of impurities into solution along with the major components of the carbonate mineral (i.e., Ca^{2+}, Mg^{2+} and CO_3^{2-}; see Eqs. (1a) and (1b)). Additional sources of metals to carbonate aquifers are non-carbonate minerals, such as oxides, clays and sulfides that were co-deposited with the carbonate, and which may contribute to release of trace elements into solution. While trace metal concentrations in calcite and dolomite minerals are generally lower than in sulfides and oxides (Barker et al., 2003; Kamber and Webb, 2007; Querol et al., 2001), carbonate minerals are more sensitive to pH variations and dissolve in larger quantities than associated sulfides and oxides under elevated partial-pressures of CO_2 (pCO_2) (e.g., Wunsch et al., submitted for publication). For example, Lu et al. (2010) and Kirsch et al. (submitted for publication) concluded that calcite or dolomite were the main sources of several trace metals in their elevated-pCO_2 experiments, even though calcite and dolomite were only minor fractions of the reacted rocks.

In previous work (Wunsch et al., submitted for publication), we evaluated metal release from natural limestone rocks at pCO_2 of 0.01, 0.1 and 1 bar and low O_2 concentrations. Calcite dissolution was the dominant geochemical reaction in these experiments and was responsible for release of several metals, including Ba^{2+}, Sr^{2+}, and Co^{2+}, into solution, albeit at concentrations that did not exceed regulatory limits. Aqueous concentrations of As in these previous experiments exceeded USEPA-mandated maximum contaminant levels (MCL) (USEPA, 2011), mainly due to desorption at 1 bar pCO_2. Concentrations of other metals, such as Ni, increased but specific release mechanisms were uncertain. In this paper, we expand this experimental work to dolomite rocks, focusing on the following questions: (1) which mineral phase is most likely to contribute to metal release based on impurity content, (2) which mineral is most likely to contribute to metal release based on mineral reactivity, and (3) which elements are released to solution and to what concentrations under elevated pCO_2 conditions? These questions were addressed by thorough characterization of the dolomite samples, batch dissolution experiments and geochemical modeling.

2. Methods

2.1. Dissolution experiments

Sevy Dolomite and Kindblade Dolomite samples were obtained from the United States Geological Survey core laboratory in Lakewood, Colorado, USA. A sample of Cotter Dolomite was obtained from a road-cut several miles south of Ozark, Missouri.

The samples were prepared and reacted with CO_2 in an experimental setup (Fig. 1) following Wunsch et al. (submitted for publication). Initially, each rock was crushed with a Boyd jaw crusher (Rocklabs Limited, Auckland, New Zealand) and sieved to achieve rock fragment sizes larger than 4 mm in diameter. After rinsing with water to remove fines, 150 g of each rock were placed in a closed polycarbonate beaker (i.e., a reactor), with an initial pure water volume of 750 ml and an N_2 atmosphere for 18 days. The partial pressure of CO_2 in the head-space of the reactors was then progressively increased from 0.01 bar to 1 bar, in stages that lasted 15 days each (Table 1). As an experimental control, 3 g of pure $CaCO_3$ powder (Sigma Aldrich, Inc.) were reacted in a fourth reactor. The reaction took place at ambient room temperature (~22 °C). The total pressure in the reactors was 1 bar and controlled by a single downstream pressure regulator (Equilibar Inc., Fletcher, North Carolina, USA), whereas partial-pressures of CO_2 and N_2 were achieved by pre-mixing these gasses in compressed tanks. Experiments were conducted in six stages (A through F) with increasing pCO_2 and decreasing pN_2 during stages B through E (Table 1). At the end of the pressurized experiment, the system was allowed to equilibrate with the atmosphere by disabling the pressure regulator and loosening the reactor lids. Four ml of aqueous samples were extracted at 3, 6 and 12 h and at 1, 2, 4, 7, 11, and 15 days from the beginning of each stage, with the exception of stage B (100% N_2), where sampling was less frequent. Pressure in the beakers was maintained during sampling. These aqueous samples were filtered and acidified for cation analysis by ICP-MS. Anion concentrations were measured by ion chromatography in 1 ml of samples taken at the end of each stage. Overall, a total of approximately 160 ml of solution were removed from each reactor for aqueous analyses by the end of the experiment. Sampled volume was not replaced with fresh water to prevent dilution. pH was measured in situ using ISFET pH probes (Campbell Scientific, Inc.). Reactor pressure and pH were recorded at 15-s intervals with a datalogger (Campbell Scientific, Inc.).

Two minor changes in the experimental setup from Wunsch et al. (submitted for publication) were implemented in the experimental design: (1) 1 L polycarbonate containers (Nalgene) were used as reactors (instead of glass), and (2) external, disposable 0.45 μm PVDF filters were used to filter the aqueous samples (instead of in situ 0.5 μm stainless-steel filters). The container mate-

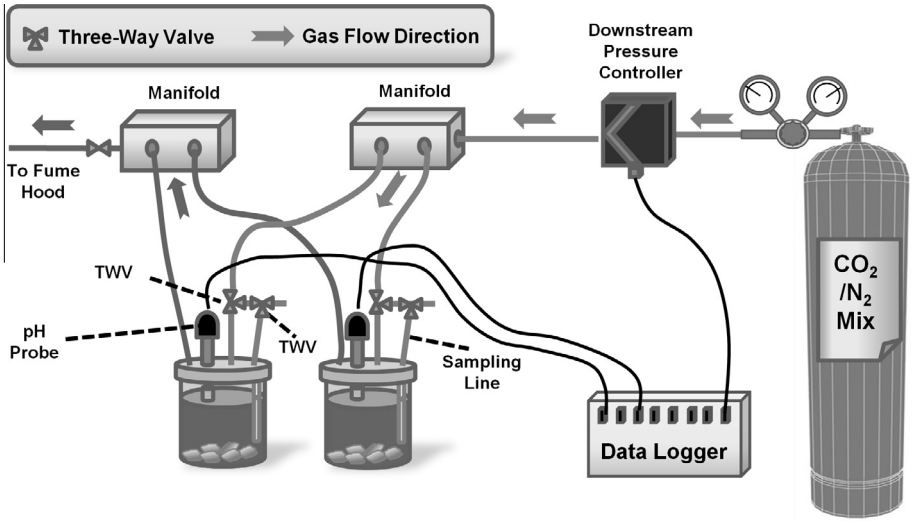

Fig. 1. Schematic of the pressurized experiment setup. TWV = Three Way Valve (modified from Wunsch et al., submitted for publication).

Table 1
Different stages of the pressurized experimental work.

	Stage					
	A	B	C	D	E	F
Stage duration (days)	9	18	15	15	15	12
Pressure (bar) above atmospheric	Atmospheric	1	1	1	1	Atmospheric
% CO_2	0.039	0	1	10	100	0.039
% N_2	78.084	100	99	90	0	78.084

rial was changed to polycarbonate to reduce potential glass dissolution during the experiment. These polycarbonate containers were harder to sealand pressure fluctuations lasting several hours were observed at day 60 of the experiment. Difficulties sealing the reactors also lead to integrity failure of the control reactor on the last day of the experiments in the 1 bar CO_2 stage. At this point the pressure in the other reactors dropped from 1.0 to 0.94 bar, resulting in an increase in 0.3–0.4 pH units due to this failure. No aqueous samples were taken from the control reactor after the failure.

2.2. Rock characterization

Mineral composition of the rock samples was determined using Quantitative Elemental Mapping (QEMSCAN) on thin sections and XRD analysis on powdered samples. The QEMSCAN method combined automated SEM point-counting at 10 μm point spacing with post-processing to determine sample mineralogy and mineral volumetric abundance. The SEM used was a Carl Zeiss EVO 50 SEM, equipped with four Bruker X275HR silicon drift X-ray detectors. Post-processing was done using the iMeasure/iDiscover software suite (FEI, Inc., Hillsboro, Oregon, USA).

XRD analysis was performed on a XDS 2000 instrument (Thermo ARL Inc. [formerly Scintag], Waltham, Massachusetts, USA). A portion of powdered sample from each rock was used for whole-rock, randomly-oriented XRD scan. Another portion was treated to remove the carbonate fraction using 1 M Na-acetate/acetic acid buffer (Jackson et al., 1950), followed by isolation of the clay fraction by the Millipore method (Moore and Reynolds, 1997). The remaining clay fraction was scanned air-dried. The clay fraction of the Cotter Dolomite was re-analyzed after glycolation because the air-dried scan produced a broad peak that suggested the presence of swelling clays The presence of kaolinite was confirmed in the Sevy Dolomite by comparing peaks from before and after heating samples at 500 °C for 2 h (Moore and Reynolds, 1997). Each sample was scanned in a 2θ angle range of 4–50°, at a scan rate of 2° per minute, with a resolution of 0.02°. DMSNT software (Thermo ARL Inc. [formerly Scintag], Waltham, Massachusetts, USA) was used for data reduction and plotting. Peak intensity data from Brindley and Brown (1980) and Moore and Reynolds (1997) was used to identify minerals. Surface area was measured on 2 g of rock chips approximately 0.5 cm in diameter (not powders) using a Micrometrics ASAP 2020 surface area analyzer with N_2 gas.

Laser ablation-inductively coupled plasma-mass spectrometry (LA-ICP-MS) analysis was performed on polished billets of each rock, to determine impurity concentrations in specific minerals. The LA-ICP-MS system consisted of a LSX-213 ablation unit with a 213 nm Nd:YAG laser (CETAC Technologies, Omaha, Nebraska, USA) connected to an Optimass 9500 Inductively Coupled Plasma-Time of Flight-Mass Spectrometer (GBC Scientific Equipment, Braeside, Victoria, Australia). Minerals were identified using a light microscope in the ablation unit, and by inspection of the major-element composition of ablated material. Elemental peaks were calibrated against NIST SRM glasses 610, 612 and 614, which have trace element concentrations on the order of 1, 50 and 500 ppm, respectively, according to Jochum et al. (2011). Ablation was done with a laser spot size of 150 μm. Internal standards used were ^{44}Ca, ^{29}Si, and ^{57}Fe for calcite, clay (kaolinite), and pyrite, respectively. Detection limits for each element were calculated as 3σ of the background for each sample run. The number of individual ablated grains for each mineral was: Dolomite: 32, 24 and 13 in Kindblade, Sevy and Cotter, respectively; Calcite: 12 in Kindblade; Pyrite: 8 in Kindblade; Clay 22 in Sevy. Not all mineral phases identified by QEMSCAN in each sample were measured by LA-ICP-MS, because the mineral phases were too small or dispersed to be identified using the integrated light microscope in the ablation unit.

Concentrations of trace elements in different fractions of the samples were also determined using the sequential extraction (SE) method of Li et al. (1995) with two adaptations for our samples. The SE included: (1) leaching of sorbed metals, (2) dissolution of carbonate fraction, where 80 ml instead of the prescribed 8 ml of sodium acetate/acetic-acid (NaOAc/HOAc) buffer was used due to the high carbonate content of the samples, (3) dissolution of metal oxides, (4) dissolution of sulfides and organic matter, and (5) dissolution of the residual fraction from the previous steps using the method of Farrell et al. (1980) where boric acid (H_3BO_3) is added to neutralize the hydrofluoric acid (HF), in order to protect glassware and the ICP-AES nebulizer. Analysis of metal concentrations in extraction products was carried out using a Perkin Elmer Optima 5300 DV ICP-AES, with the multi-element inorganic standards CCV-1 Solution A™ and CCV -1 Solution B™ (High-Purity Standards, Inc.) for reference. In addition, results from the HF digestion (residual fraction extraction) were corrected against a blank that was prepared during the digestion.

All of the analyses were performed at the Colorado School of Mines, in Golden, Colorado, USA, with the exception of the LA-ICP-MS work, which was performed at Towson University, Towson, Maryland, USA, and the HF-digestion step of the sequential extraction, which was performed at the University of Colorado, Boulder, Colorado, USA. Aqueous samples from the pressurized experiments were also analyzed at the University of Colorado at Boulder.

2.3. Geochemical modeling

Equilibrium and kinetic geochemical calculations were performed using the geochemical code PHREEQC (Parkhurst and Appelo, 1999). The thermodynamic constants used in this work were taken from the Lawrence Livermore National Laboratory (LLNL) thermodynamic database. Equilibrium models were constructed with various mineral assemblages, containing different combinations of calcite, dolomite, disordered dolomite and gypsum. The abundances of minerals initially present in the simulations were based on volumetric estimates from the QEMSCAN analysis (Table 2). Mineral masses were calculated from the volumetric estimates (in 150 g of rock) by:

$$M_i = \frac{V_i \times \rho_i}{\sum_i^n V_i \times \rho_i} \times 150 \quad (2)$$

where M_i is the mass of mineral i, and V_i and ρ_i are the volume and density, respectively.

The mineral molar amounts represent the initial conditions of geochemical simulations and were also used in calculation of saturation indices. In specific cases, we applied minor adjustments to the estimates of the amount of gypsum initially present (discussed later). Modeling results were then compared to observed aqueous concentrations of Ca^{2+}, Mg^{2+} and pH after 15 days of reaction at each stage (a period long enough to reach equilibrium with respect to calcite and dolomite).

Kinetic simulations of dolomite dissolution were performed by programming the dissolution rate law from Palandri and Kharaka (2004) into PHREEQC:

$$\frac{dm}{dt} = -SA\left[k_{acid} \times \exp\left(-\frac{Ea_1}{R_g(T-298.15)}\right) \times \{H^+\}^a + k_{neutral} \times \exp\left(-\frac{Ea_2}{R_g(T-298.15)}\right) + k_{carbonate} \times \exp\left(-\frac{Ea_3}{R_g(T-298.15)}\right) \times pCO_{2(g)}^c\right]\left(1-\frac{IAP}{K_{eq}}\right) \quad (3)$$

where SA (m^2) is the total mineral surface area in the experiment, k_{acid}, $k_{neutral}$, $k_{carbonate}$ (mol/m^2/s) are rate constants for the acid, neutral and carbonate dissolution mechanisms. a and c (unitless) are fitting parameters, Ea is activation energy (J/mol) of each dissolution mechanism, R_g is the gas constant (8.314 J/K/mol), T is the temperature (K),{} denotes activity of solutes, IAP denotes the ion activity product and K_{eq} the equilibrium constant of dolomite. Palandri and Kharaka (2004) report fitted values to dolomite dissolution data from Busenberg and Plummer (1982) of: $\log k_{acid} = -3.76$, $\log k_{neutral} = -8.60$, $\log k_{carbonate} = -5.37$, $a = c = 0.5$, $Ea_1 = 57.6$, $Ea_2 = 95.3$ and $Ea_3 = 45.7$ J/mol.

Rate law parameters were optimized to match experimental Ca^{2+} and Mg^{2+} concentrations using the optimization code UCODE (Poeter et al., 2005). The optimization was an iterative process, whereby PHREEQC simulation results were compared to the Ca^{2+} and Mg^{2+} concentrations measured during the experiments and then values of parameters in the rate laws were incrementally adjusted by UCODE (up to 2% change from the previous value). Subsequently, PHREEQC was re-run with the adjusted parameters and simulation results compared to experimental data (see Skold et al., 2007, for a comprehensive overview of UCODE-PHREEQC coupling). This process was repeated until the sum of weighted-squared-residuals with respect to parameter values reached a minimum, after which the parameters were considered optimized. The criteria for optimization convergence was <1% fractional change for all parameters. Concentrations of both Ca^{2+} and Mg^{2+} were given equal weights during optimization and calculations of sum of weighted-squared-residuals. The last two measurements of Mg^{2+} in the 1 bar pCO_2 stage were not representative of dolomite dissolution (as explained in Section 3.2.2) and therefore omitted from the optimization. Sensitivity analyses and optimizations were performed using the log-transformed values of parameters with initial or expected small values, to compensate for bias caused by orders-of-magnitude differences and for ease of calculation (Hill, 1998). Optimization was performed in several stages. First, the dolomite dissolution rate was implemented as reported in Palandri and Kharaka (2004) with total surface area as the only optimized value. Second, a sensitivity analysis was run on all rate law constants reported by Palandri and Kharaka (2004), excluding activation energies (simulations were run at 22 °C, close to the reference temperature of 25 °C for which the fitting parameters were calculated) but including total surface area. Then, the optimization process was re-run by varying only the parameters that the results proved most sensitive to.

3. Results

3.1. Rock properties

3.1.1. Mineralogical composition and textural description

QEMSCAN and XRD analyses confirmed that dolomite was the dominant carbonate mineral in all three rocks (Figs. 2 and 3, Table 2). However, the different rocks contained different abundances of major, minor and trace minerals, as detailed below. Metal oxides could not be readily quantified using XRD and QEMSCAN. However, the presence of oxides cannot be ruled out as Fe was detected in the oxide fraction of the SE analysis (Table 2). Pyrite was detected only in trace amounts in all rocks using QEMSCAN (Table 2). Concentrations of oxides and pyrite were estimated from Fe concentrations in the oxide and sulfide fractions following the SE analysis, respectively (Table 2). Several tens of ppm of S were detected in the sequential extraction in the SE "sorbed" fraction of all three rocks which may indicate the presence of gypsum.

3.1.1.1. Kindblade Dolomite. In addition to dolomite, the Kindblade Dolomite contained minor amounts of calcite, mostly in distinct, white veins, and trace amounts of quartz, feldspar, and pyrite (Fig. 2a). The percentage of clay minerals detected in the QEMSCAN

Table 2
Mineralogical composition of the natural rock samples, based on thin section EDS analysis (QEMSCAN).

	Kindblade Dolomite		Sevy Dolomite		Cotter Dolomite	
	Vol%	Mass, ppm	Vol%	Mass, ppm	Vol%	Mass, ppm
Quartz	2.16	20,313	57.22	558,069	19.08	178,036
Dolomite[a]	74.93	754,226	36.41	280,540	78.41	784,257
Calcite	6.61	130,880[b]	0.04	5932[b]	0.08	15,800[b]
Calcite (Mg-bearing)[c]	6.68		0.54		1.53	
Clay	8.91	86,812[d]	5.65	54,078[e]	0.81	7863[d]
Feldspar	0.54	5,105	0.05	82	0.05	13,545
Anhydrite/gypsum	0.02	163	0.01	57	0.01	83
Apatite	0.01	76	0.03	303	0	19
Pyrite	0.08	1332 (204[f])	0.02	329 (1549[f])	0	4 (118[f])
Others	0.07	1093 (300[g])	0.04	610 (5176[g])	0.03	393 (1161[g])
BET surface area (m^2/g)	0.1583 ± 0.0013		0.4917 ± 0.0031		0.3338 ± 0.0006	

[a] Ca-, Mg- and O-rich minerals with Ca/Mg ratios of roughly 1–1.47 were classified as dolomites (carbon was used to coat the carbonate samples and therefore excluded from calculations of mineral composition).
[b] Sum of "calcite" and "Mg-bearing calcite".
[c] Calcites with Ca/Mg ratios of roughly 1.48–27.57 were classified as "Mg-bearing calcites".
[d] Based on average illite density (2.75 g/cm^3).
[e] Based on average kaolinite density (2.6 g/cm^3).
[f] Mass based on Fe concentrations in the SE sulfides fraction.
[g] Mass based on Fe concentrations in the SE oxides fraction, assuming Fe present as goethite.

analysis of Kindblade was 8.9% (vol%). However, clay minerals were not detected in the XRD data, even after removal of the carbonate fraction (see Section 2.2, Fig. 3a) and lowering the XRD scan rate. Upon closer inspection, the clay identified in the QEMSCAN of the Kindblade Dolomite only appeared as single pixels (spot size) and with the pixels widely dispersed throughout the sample (Fig. 2a), which may point to false identification of clays by the QEMSCAN along mineral boundaries. Kindblade also had low over-

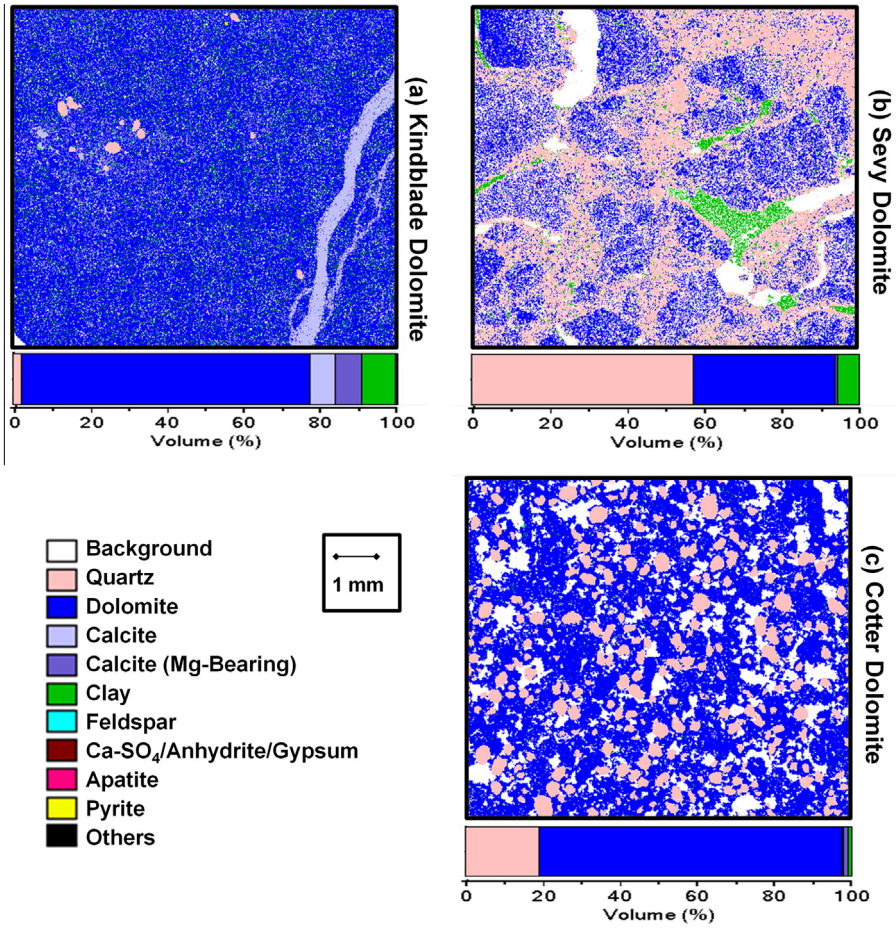

Fig. 2. False-color maps of mineral distribution in the (a) Kindblade Dolomite, (b) Sevy Dolomite and (c) Cotter Dolomite obtained from QEMSCAN analysis. (For interpretation of the references to colour in this figure legend, the reader is referred to the web version of this article.)

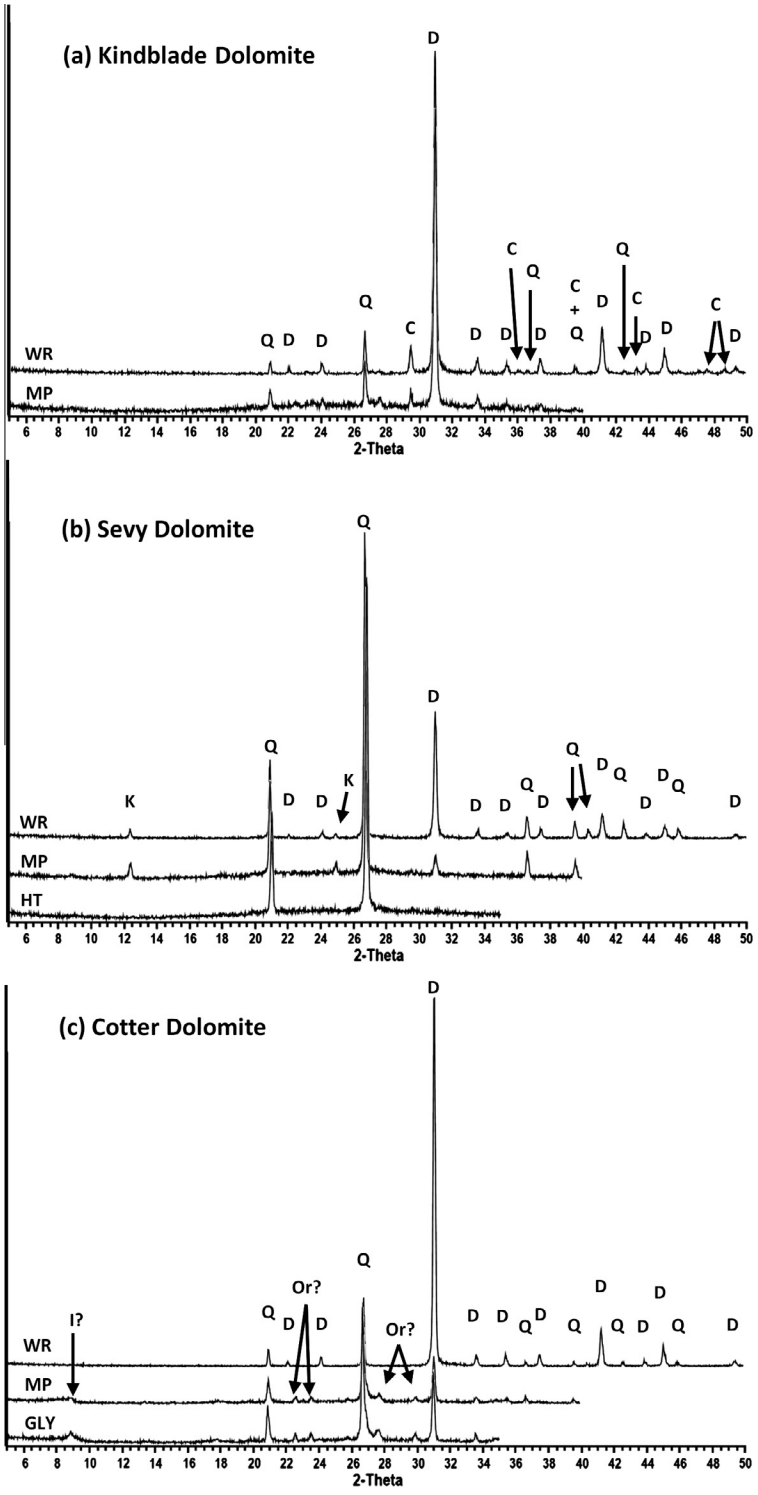

Fig. 3. X-ray diffraction (XRD) patterns of the (a) Kindblade Dolomite, (b) Sevy Dolomite and (c) Cotter Dolomite. Superimposed XRD patterns correspond to: WR – Whole Rock (randomly-oriented powdered sample), MP – Millipore (scan after dissolution of carbonate fraction and isolation of clay fraction using the Millipore method), HT – Heat Treatment (post-Millipore and heating to 550 °C), GLY – Glycolation (post-Millipore and desiccation in ethylene glycol atmosphere). Scans HT and GLY were performed as needed for specific rocks, as detailed in Section 2.2. Mineral identification abbreviations are as follows: Q – Quartz, C – Calcite, D – Dolomite, K – Kaolinite, I – Illite, Or – Orthoclase/Anorthoclase.

all surface area of the bulk rock compared to the other samples (Table 2), which is consistent with a rock with low clay concentrations. The Kindblade rock contained the most pyrite among the rocks according to the QEMSCAN analysis, and pyrite crystals were observed in this rock using the optical microscope of the LA-ICP-MS. In contrast, Kindblade had the second-most pyrite based on Fe abundance in the sulfide fraction of the SE analysis (Table 2).

3.1.1.2. Sevy Dolomite. Quartz was the most abundant mineral in the Sevy sample (52.2 vol%), followed by dolomite grains

Table 3
Elemental abundances in dolomite and calcite grains (LA-ICP-MS analysis). Concentrations are averages of multiple grains, as indicated in the "detected" columns (BDL = below detection limit).

	Kindblade Dolomite				Sevy Dolomite		Cotter Dolomite	
	Dolomite		Calcite		Dolomite		Dolomite	
	Conc. (ppm)	Detected (/32)	Conc. (ppm)	Detected (/12)	Conc. (ppm)	Detected (/24)	Conc. (ppm)	Detected (/13)
Mn	59.37	32	13.21	12	157.56	24	254.07	13
Co	2.70	31	0.25	12	4.06	24	0.77	13
Ni	12.50	32	2.57	12	30.77	24	5.13	13
As	2.80	29	0.30[a]	1	12.27	14	0.76	8
Sr	131.95	32	141.89	12	99.88	24	83.07	13
Tl	0.23	22	0.04	7	0.64[a]	1	0.10	13
Zn	8.73	32	0.66	12	14.87	24	5.22	13
Mo	7.49	31	0.72[a]	1	3.80	6	BDL	0

[a] Mostly BDL.

(36.4 vol%). The Sevy rock also contained clay, primarily kaolinite based on XRD peak identification (Figs. 2b and 3b). Sevy contained the most pyrite based on Fe abundance in the sulfide fraction of the SE analysis (Table 2). It was also richest in metal oxides based on Fe concentrations in the oxide fraction of the SE.

3.1.1.3. Cotter Dolomite. The Cotter Dolomite had a clastic texture, with dolomitic cement between dolomite and quartz grains, and only trace amounts of other minerals (Table 2, Figs. 2c and 3c). One clay peak was identified in Cotter using XRD. This peak correlated to either illite or glauconite; other clay peak intensities were too low to identify definitively (Fig. 3c). The Cotter Dolomite had the lowest concentration of metal oxides and sulfides based on both the QEMSCAN and SE analyses.

3.1.2. Distribution of trace elements: sequential extraction

The SE analysis provided insight into the mineral pool that hosted the most impurities in each rock (Fig. 3, Supplemental Material 1). It should be noted that the detection limits of elements in the carbonate fraction (in ppm of rock) were approximately two orders of magnitude higher than those of the other fractions, due to the addition of relatively large amounts of reagent in the carbonate dissolution process (see Section 2.2, Supplemental Material 1). Similarly, the detection limits of elements in the residual fraction were approximately one order of magnitude higher than that of the other fractions (excluding carbonate), because HF-digested samples were diluted by a factor of 10 prior to ICP-AES analysis. Higher detection limits in the carbonate fraction may lead to underestimation of impurity content compared to the other fractions. However, where results were below detection limit in the carbonate fraction, LA-ICP-MS analysis provided trace element concentrations of the carbonate fraction. The main observations from the SE analysis are as follows:

- Sevy contained the highest overall concentrations of As, Ba, Cd, Co, Cr, Fe, Mn, Ni, Pb, S, Sr, Ti, and Zn (Fig. 3, Supplemental Material 1). Kindblade contained the most Li and Mo. Se was found mostly in the Cotter rock.
- Concentrations of Tl, U, Sn, and Sb were below detection limits in all rocks.
- The carbonate fraction was the primary host of minor and trace elements in the samples as follows: As (Kindblade), Ba (all rocks), Cd (Kindblade, Cotter), Cr (Kindblade, Cotter), Li (all rocks), Mn (Kindblade), Pb (Cotter), Se (Sevy, Cotter) and Zn (Kindblade, Cotter).
- Several elements were found sorbed in appreciable amounts relative to the total concentrations in the rock (>5%): As (Cotter), Co (Cotter), Mo (Kindblade), Ni (all rocks), and Se (Kindblade, Sevy).
- The sulfide mineral fraction of Sevy contained a significant proportion of many minor and trace elements of interest (e.g., As, Co, Mo), even though the overall abundance of sulfide minerals was low (Table 2).

3.1.3. Distribution of trace elements – LA-ICP-MS

Dolomite and quartz minerals were analyzed for metal impurities using LA-ICP-MS. Calcite in a vein and pyrite in the Kindblade sample, as well as kaolinite in the Sevy sample, were also analyzed using LA-ICP-MS. The LA-ICP-MS results for dolomite minerals were generally in good agreement with the SE analysis of the carbonate fractions of the different rocks. The main observations from the LA-ICP-MS analysis are as follows:

- Dolomite minerals in the Sevy rock contained, on average, more Co, Ni, As, Nb, Cs, U and Zn than dolomite minerals in other rocks (Table 3; Supplement Material 2). Sm, Ge and Eu concentrations in dolomite minerals of Sevy were the highest, yet these elements were only detected in a few ablated minerals. The Kindblade dolomite minerals were richest in Ba, Mo, Sr, Tl and Pb. The Cotter dolomite minerals contained the highest concentrations of Mn compared to the other dolomites.
- The Kindblade dolomite minerals had higher impurity concentrations, per ablated mass, than Kindblade calcite minerals, with the exception of Sr. Also, Kindblade pyrites contained higher impurity concentrations than any other ablated mineral across all three rock samples, most notably of Mn, Co, Ni, Ge, As, Tl and Pb.
- Almost all minor and trace elements, apart from Co and Ni, were below detection limit in the kaolinite minerals of the Sevy rock.

3.2. Pressurized experiments

3.2.1. pH

Temporal changes in pH reflected the boundary conditions imposed during different stages of the experiment. When the system was purged with N_2, and $pCO_2 \approx 0$, pH increased to >9 (Fig. 5a). During this stage, pH readings were not steady in the Kindblade reactor due to severe pressure leaks, which were fixed before transitioning to the next stage. Upon increase in pCO_2, pH dropped to a minimum value for that stage (6.73–6.8 in Stage C, 6.1–6.29 in Stage D, 5.53–5.73 in Stage E) within a few hours, then increased slowly over the course of several days by ~0.5 pH units, indicating acidity buffering through mineral dissolution. The buffering capacities of the different rocks were overall similar, despite the different mineralogical compositions and perhaps dissolution of different reactive minerals (see Section 4.1).

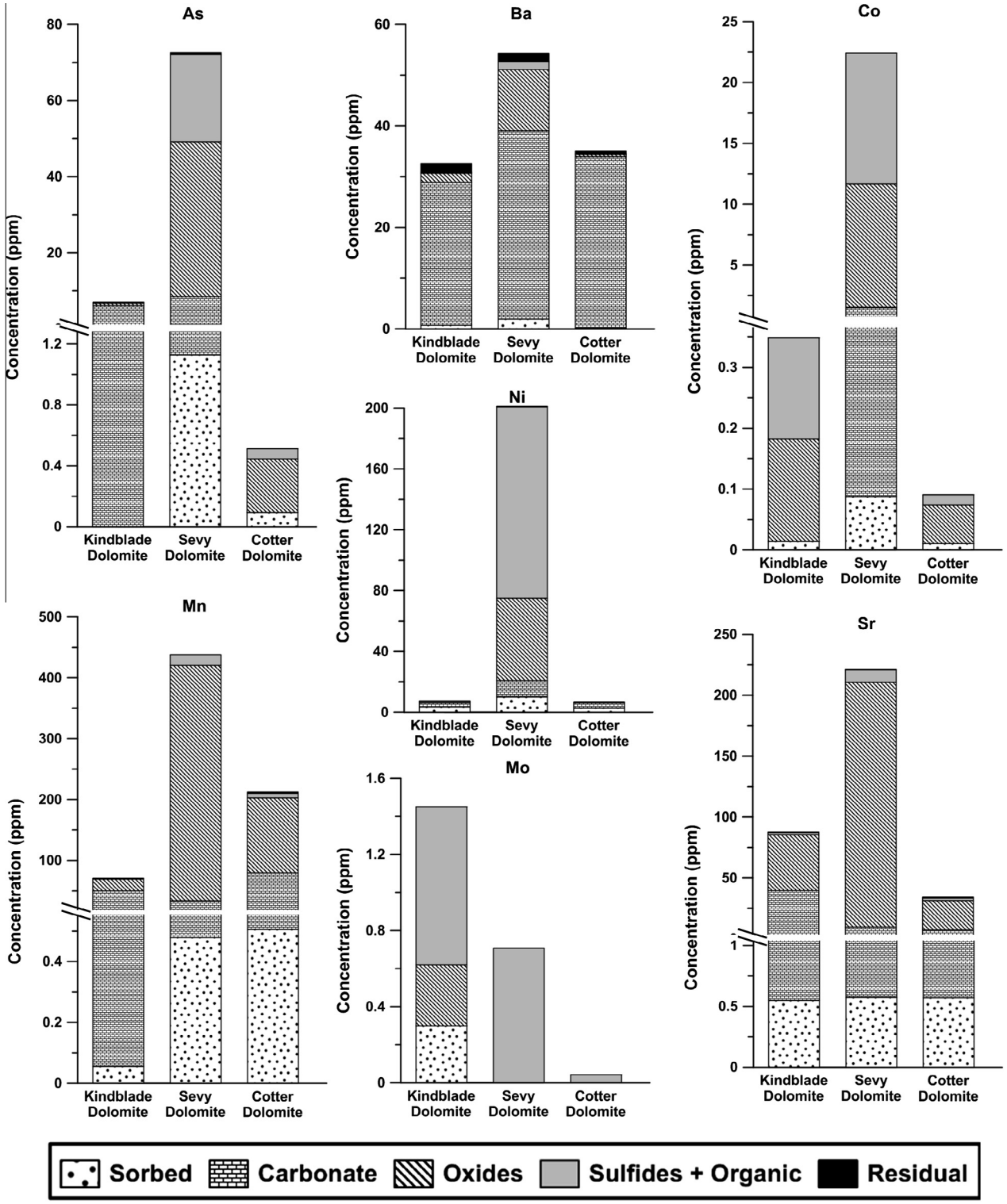

Fig. 4. Selected results of elemental abundances in different mineral fractions (sequential extraction procedure). Concentrations refer to abundance in the whole rock. Notice the break and change of scale in the *y*-axes of As, Co, Mn and Sr plots.

3.2.2. Release of major elements

Concentrations of Ca and Mg increased rapidly at the beginning of stages C through E, then approached a constant value towards the end of each stage (Fig. 5b and c). Noticeable declines in Mg^{2+} concentrations were observed in the reactors containing natural rock samples around day 60, which we attribute to the unexpected pressure fluctuations in the system at that time. Interestingly, Ca^{2+} concentrations were not affected by the pressure fluctuations, which may rule out carbonate precipitation as the mechanism that led to decreases in Mg^{2+} concentrations (given that magnesite precipitation rates are much slower than that of calcite; Saldi et al., 2009). Also, Ca^{2+} and Mg^{2+} exhibited opposite trends during system decompression: Ca^{2+} concentrations decreased while Mg^{2+} concentrations increased. Concentrations of SO_4^{2-} generally remained

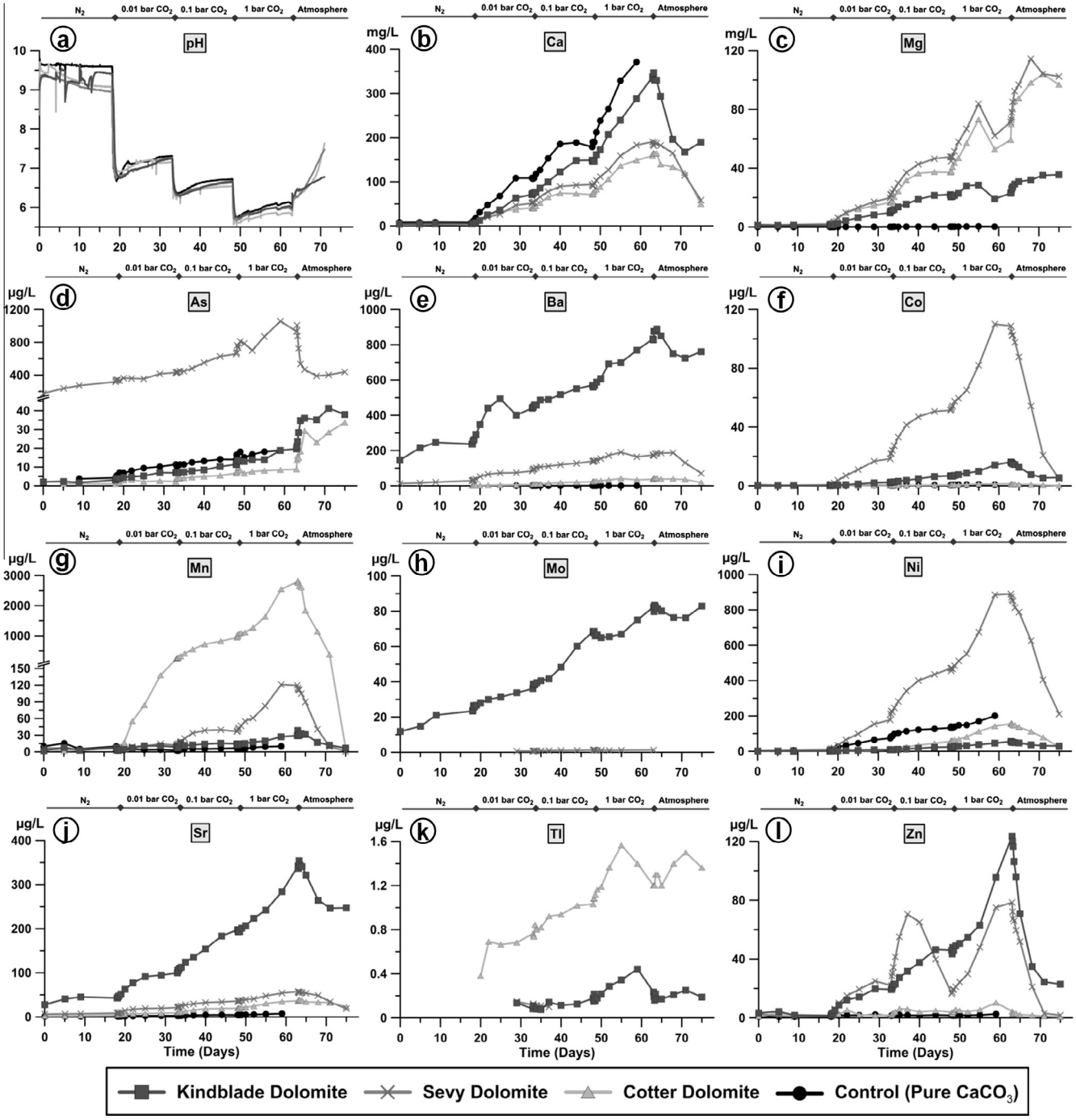

Fig. 5. pH and aqueous concentrations of metal as a function of time throughout the pressurized experiments.

<6 mg/L (not shown); the low sampling frequency did not allow us to determine a particular trend.

3.2.3. Release of minor and trace elements

Aqueous concentrations of many elements increased during the experiment, including As, Ba, Co, Cs, Ge, Mn, Mo, Ni, Rb, Sb, Sr, Tl and Zn (Fig. 5; Supplemental Material 3). Aqueous concentrations of several trace elements increased, but remained <1 µg/L, including Ce, Eu, La, Nd, Ru, Sm, U, Y and Zr. Aqueous concentrations of Pb did not exhibit a particular trend, and remained <0.5 µg/L. The Kindblade Dolomite released the most Ge, Sr, Ba, Sm and Eu, while the Sevy Dolomite released the most Co, Ni, As, Cs and U. The Cotter Dolomite was the least dominant source of metals, yet released Mn into solution in concentrations that were significantly higher than in the other reactors. The Cotter Dolomite also released the most Tl. During the decompression stage (Stage F), some elements decreased in concentrations (Ba, Ce, Co, Ge, La, Mn, Nd, Ni, Ru, Sr, Y, Zn, Zr) while others increased (Cs, As in the Kindblade and Cotter reactors). Aqueous concentration trends of As and U varied among rocks during decompression.

Aqueous concentrations of As and Ni in the control reactor were comparable with concentrations in reactors that contained the dolomite rock samples. These high aqueous concentrations probably resulted from the high As and Ni concentrations of 197.7 and 9.5 ppm, respectively, that were found in the control $CaCO_3$. Therefore, we regard the aqueous As and Ni concentrations in the

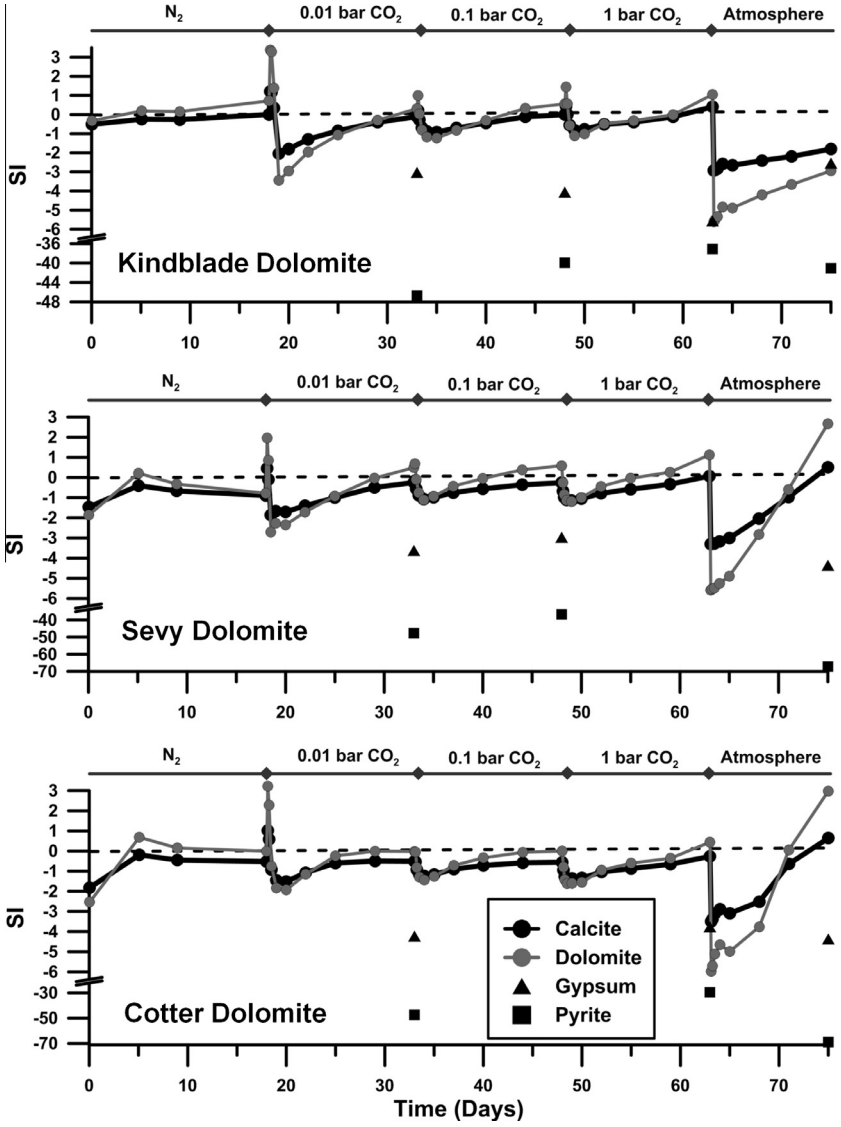

Fig. 6. Saturation indices (SIs) calculated for calcite, dolomite, gypsum and pyrite in each reactor. Pyrite and gypsum SIs were only calculated where sulfate was measured, at the end of each stage. In some instances sulfate was BDL, therefore calculation of pyrite and gypsum SIs were not possible.

Kindblade and the Cotter reactors as genuine. However, As concentrations in the Sevy reactor were exceptionally high from the beginning of the pressurized experiment, even before reaction with CO_2, and may be a result of unknown contamination. Furthermore, the Sevy Dolomite did contain high concentrations of sorbed As (Fig. 4). It is therefore possible that As desorbed in this rock upon contact with initially-pure water (Radu et al., 2005).

4. Discussion

4.1. Calcite and dolomite dissolution with increased pCO_2

The observed trends of Ca^{2+} and Mg^{2+} can be attributed to dissolution of carbonate minerals, which approached equilibrium towards the end of each stage according to saturation index (SI) calculations (Fig. 6). Simulated equilibrium concentrations of Ca^{2+}, Mg^{2+} and acidity following mineral dissolution were compared to observed concentrations at the end of each stage (after 15 days of reaction). We did not expect a good fit to data at the end of the 1 bar CO_2 stage due to the pressure drop that occurred shortly before sampling. Nonetheless, the mineral assemblages that produced model results closest to observed data were consistent with minerals detected in the QEMSCAN analysis: dolomite alone (Cotter), dolomite and gypsum (Sevy) and dolomite and calcite (Kindblade) (Fig. 7). The co-dissolution of calcite and dolomite in the Kindblade reactor is apparent in the higher concentrations of Ca^{2+}, and lower concentrations of Mg^{2+} compared to other reactors (where calcite dissolution was not significant) (Fig. 8a). According to equilibrium simulations, calcite dissolves ~14 times more than dolomite (on a molar basis) when both minerals are present, even when calcite is much less abundant than dolomite. However, based on the observed Ca:Mg ratio in solution (Fig. 8a) it is likely that calcite only dissolved ~3 times more than dolomite in the Kindblade reactor (this value could be lower if the dolomite minerals in the Kindblade Dolomite were Mg-poor, and higher if some Mg^{2+} emerged from solid-solution in calcite during dissolution). The difference between the equilibrium simulations and calculated masses of calcite and dolomite that dissolved in the Kindblade reactor can be explained by the low surface area of calcite, predominately confined to veins, that was available for reaction compared to that of dolomite. Surface area considerations are not included in the equilibrium simulations. Regardless of the exact

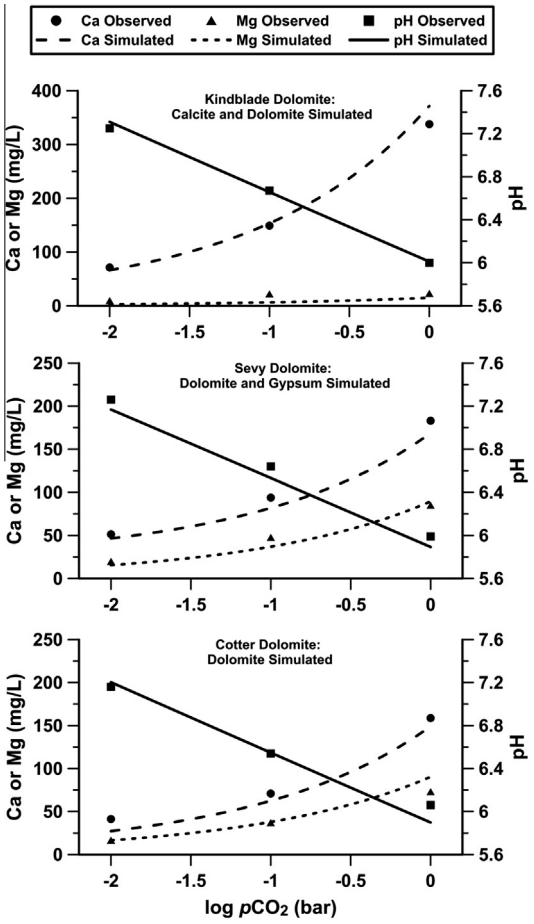

Fig. 7. Comparison of experimental aqueous Ca, Mg and pH (symbols) to results from equilibrium simulations (lines).

amount of calcite that dissolved in the Kindblade reactor, the relatively low Ca-to-Mg ratio is expected due to a preferential dissolution of calcite over dolomite resulting from the inhibiting effect of high Ca^{2+} concentrations on dolomite dissolution (Busenberg and Plummer, 1982; Pokrovsky and Schott, 2001). Finally, the acidity-buffering response of each rock was similar, regardless of whether dolomite or calcite was the main buffering agent.

4.2. Sources of minor and trace elements

To investigate the sources of metals to aqueous solution in the experiments, we compare aqueous concentrations of metals to the solid-phase metal distribution from SE and LA-ICP-MS analyses. Let us take Sr^{2+}, for example. Sevy contained the highest total soild-phase Sr concentrations, and the highest Sr concentrations in the oxide and sulfide fractions (see Supplement Material 1, Fig. 4). If total rock dissolution, or dissolution of oxides and sulfides, controlled Sr release we would expect aqueous Sr^{2+} concentrations to be highest in the Sevy reactor. Similarly, all three rocks contained approximately the same amount of sorbed Sr, thus we would expect similar aqueous concentrations in all reactors if desorption were controlling Sr release to solution. However, the highest aqueous Sr^{2+} concentrations were observed in the Kindblade experiment. The dolomite phase in the Kindblade Dolomite contained higher Sr concentrations than dolomite grains in the Sevy and Cotter samples (Table 3). Increased Sr^{2+} concentrations are highly correlated to increased Ca^{2+} concentrations, leading to the interpretation that carbonate mineral dissolution is the dominant mechanism for Sr release to solution (Fig. 8b). It is not surprising that carbonate mineral dissolution is the dominant release mechanism for Sr, which has long been known to substitute for Ca in the calcite and dolomite lattices (e.g., Bowen, 1956; Kulp et al., 1952).

Mn provides another example. Sorbed Mn concentrations were similar in all three rocks and Sevy contained the highest concentrations of Mn in the oxide and sulfide fractions. However, the highest aqueous Mn^{2+} concentrations were observed in the Cotter reactor (Fig. 8c). Amongst the three rocks, Cotter had the highest Mn concentration in the carbonate fraction (Fig. 4, Table 3). In addition, aqueous Mn^{2+} concentrations correlated well with aqueous Ca^{2+} concentrations. These observations lead to the interpretation that carbonate dissolution was also the dominant release mechanism for Mn^{2+}.

Other trace elements can also be associated with the carbonate mineral pool. Co concentrations in the carbonate fraction were below the detection limit of the SE procedure in all rocks, yet Co was found in dolomite and calcite minerals using LA-ICP-MS. The relative enrichment of Co among dolomite minerals in all rocks, as well as correlations between Co^{2+} and Ca^{2+} concentrations (Fig. 8d), support carbonate mineral dissolution as the major release mechanisms for Co in these experiments. All three rock samples released Ni into solution in accordance with the relative abundance of Ni in both the carbonate and oxide mineral fractions of the rocks. However, correlation between aqueous Ni^{2+} concentrations and Ca^{2+} concentrations (Fig. 8e) suggests that carbonate mineral dissolution was again the main release mechanism of Ni into solution. Aqueous Tl^{+} correlated well with aqueous Ca^{2+} in the Cotter reactor, and to a lesser extent in Kindblade reactor (Fig. 8) It is possible that some Tl in the Kindblade and Cotter reactors was released from sorption sites in pyrite, similar to limestones investigated by Wunsch et al. (submitted for publication). However, the calcite- and dolomite-bound concentrations of Tl (assuming preferential dissolution of calcite in the Kindblade Dolomite) are consistent with the relative amounts of Tl^{+} in solution.

Trends of Zn^{2+} release were inconsistent among the reactors. Aqueous concentrations of Zn^{2+} correlated with Ca^{2+} concentrations in the Kindblade reactor (Fig. 8g), which can be interpreted as Zn release through carbonate-mineral dissolution. Interestingly, trends in Zn^{2+} increase were not consistent in all stages of the Sevy Dolomite dissolution (Fig. 5l): Zn^{2+} concentrations decreased approximately 7 days into the 0.1 bar pCO_2 stage. The reason for the decrease is unknown, however, the stages of increase correlate very well to Ca^{2+} increase in the Sevy reactor, suggesting a carbonate mineral source. Aqueous Zn^{2+} concentrations in the Cotter and control reactors were similar and probably represent experimental background. Aqueous concentrations of Mo^{2+} in the Kindblade reactor were up to 60 times higher than in the Sevy reactor (Fig. 5h), yet Mo abundance in the sulfide fractions of the Kindblade and Sevy Dolomites were similar (Fig. 4). LA-ICP-MS data indicated that Kindblade dolomite grains contained more Mo than Sevy dolomite grains, yet the correlations between Mo^{2+} and Ca^{2+} was not very robust compared to other elements ($R^2 < 0.9$, not shown). In this case, Mo aqueous concentrations can be explained by a combination of release by calcite dissolution and the presence of Mo in the sorbed fraction of Kindblade.

4.3. Kinetic simulations

Equilibrium simulations suggested that dolomite was the main source of aqueous concentrations of Ca^{2+} and Mg^{2+} in the Cotter Dolomite reactor (see Section 4.1). We therefore used aqueous data from the Cotter reactor as reference for optimizing the rate law from Palandri and Kharaka (2004). In the first optimization attempt, only surface area was allowed to vary. Overall, the fit of the original parameters from Palandri and Kharaka to experimental

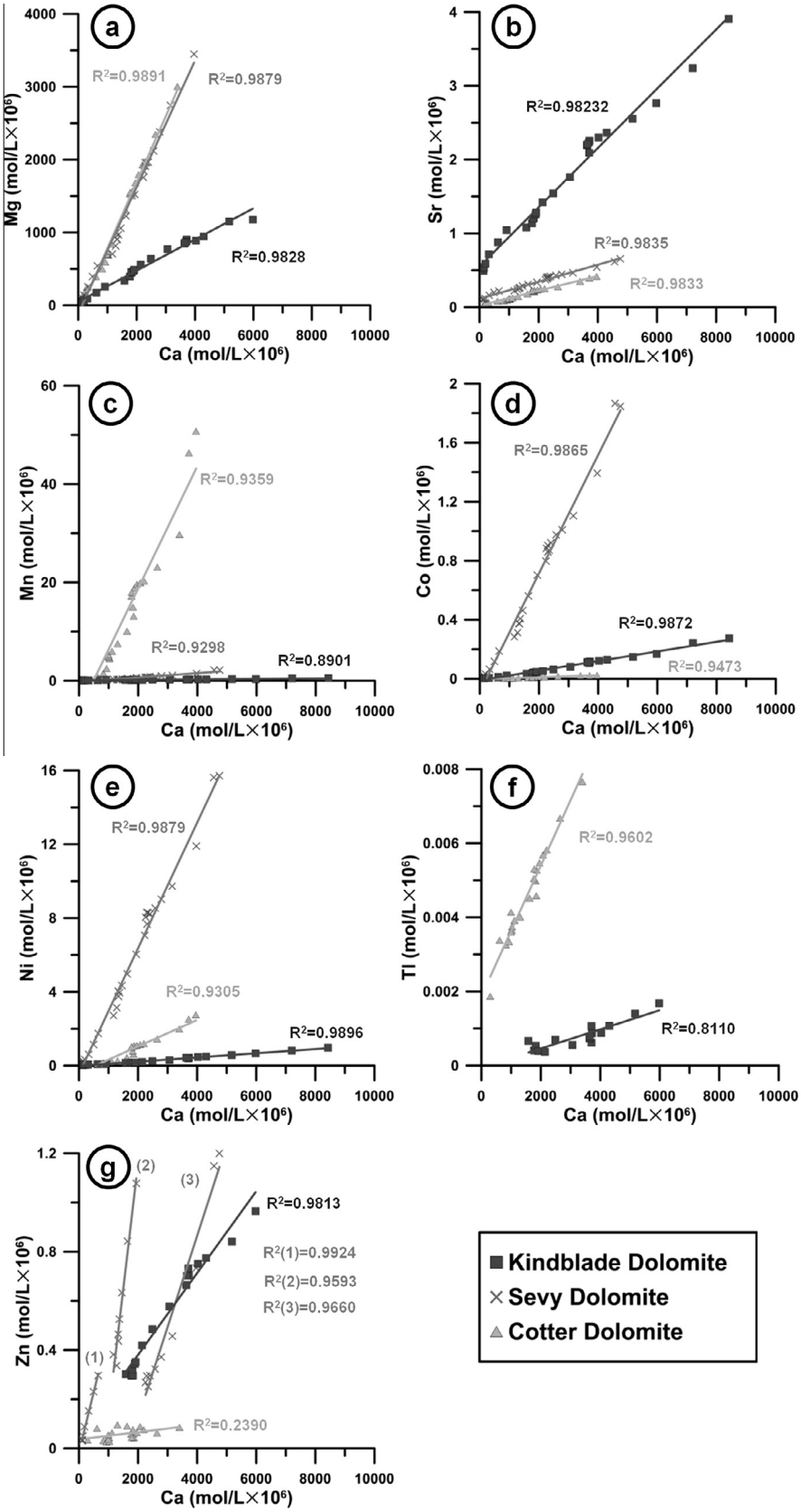

Fig. 8. Correlation of Mg and trace metal concentrations to Ca concentrations in solution.

data was reasonable, with fit-to-data $R^2 = 0.962$ (Fig. 9, upper panel). In addition, the simulated pH matched the observed pH quite well, even though pH data was not included in the optimization. However, the fit was achieved only by assigning a dolomite surface area that was 5 orders of magnitude lower than the measured BET surface area (Table 2).

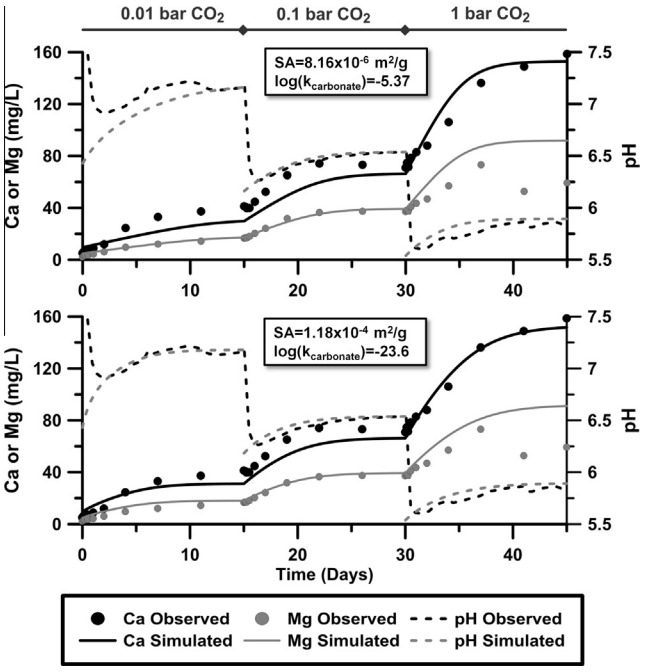

Fig. 9. Comparison of kinetic dolomite dissolution simulations and observed Ca, Mg and pH from the pressurized experiments. See Section 2.3 for definition of parameters.

It is generally expected that addition of more parameters to an optimization attempt would result in a better fit. At the same time, it is practical to focus on the few most-sensitive parameters that, when varied, lead to greater impact on simulation results. Sensitivity analysis revealed that results were most sensitive to variations in $\log(k_{carbonate})$, followed by surface area. Therefore, only these two parameters were allowed to vary in the second optimization. The addition of $\log(k_{carbonate})$ to the optimization process had a dual effect: not only the R^2 of the fit improved slightly to 0.978 (Fig. 9, lower panel), but the calculated reactive surface area of dolomite was two orders of magnitude higher than in the previous optimization. Still, the optimized surface area was three orders of magnitude lower than the measured BET surface area. The difference between the optimized values and the BET values is perhaps not surprising. For example, White and Peterson (1990) report reactive surface area to be 1–3 orders of magnitude smaller than the total surface area (measured BET).

The exercise of fitting an existing kinetic rate law to experimental data resulted in several interesting observations: (a) The most sensitive parameter in the dolomite dissolution rate law is $\log(k_{carbonate})$, representing the carbonate mediated dissolution mechanism. The proton mediated dissolution mechanism ($\log(k_{acid})$) has only minor importance in predicting dolomite dissolution. Pokrovsky et al. (2005) demonstrated that dolomite dissolution rates were strongly dependent on pCO_2 at low pCO_2 values (<10 atm). In a later paper, Pokrovsky et al. (2009) were able to explain much of the variability in their dolomite and calcite dissolution experiments simply by fitting dissolution rates to second-order polynomials, where the only independent variable was pCO_2. (b) Previously published rate laws and fitted parameters should be used with caution. Use of dolomite dissolution rate from Palandri and Kharaka (2004) and the measured BET, with no optimization, resulted in very fast dissolution of dolomite and almost instantaneous (~10 min) establishment of new steady-state conditions in our simulations. Both optimization attempts resulted in reactive surface areas that were several orders of magnitude lower than the measured BET value for the Cotter Dolomite, a phenomenon linked to selective reactivities associated with different types of surface sites (e.g., Washton et al., 2008), inactivity of etch pits that develop initially during early stages of dissolution (e.g., Gautier et al., 2001; MacInnis and Brantley, 1992) and presence of coatings on mineral surfaces (e.g., Cubillas et al., 2005). Whether one or two parameters were varied during the optimization, the overall fit to data was largely similar (Fig. 9), whereas the resulting "optimized" surface areas differed by two orders of magnitude. In other words, results of optimization of reaction rate laws may not be unique, because some parameters may be correlated.

4.4. Implications for drinking water

Aqueous concentrations of most minor or trace elements did not surpass USEPA (USEPA, 2011) or State of California (California Code of Regulations, 2011) regulatory limits for drinking water quality. Exceptions are shown in Table 4: As, Mn, and Ni exceeded regulatory limits, while Tl exceeded the USEPA maximum contaminant level goal (MCLG), but not the maximum contaminant level (MCL) (Table 4). It is likely that these concentrations would be lower in an actual aquifer due to dilution, dispersion, CO_2 degassing (discussed in more detail below) and reactions that result in loss from the aqueous phase during transport down-gradient of a CO_2-influenced zone.

A key finding of this study is that the increase in concentrations of most elements could be attributed to dissolution of the carbonate phase. Therefore, characterization of the trace element composition of the carbonate fraction of any rock should be an important step in risk assessment analysis of potential aquifer contamination due to CO_2 leaks. The variance in elemental and mineralogical composition among the Dolomite rocks studied here and resulting variance in aqueous chemistry point to the importance of site-specific geochemical characterization when looking at the susceptibility of trace metal contamination.

Opening of the reactors and exposure to ambient atmospheric conditions provides some insight into how groundwater quality might recover once a leak is stopped. During this decompression phase of the experiment, Ca^{2+} concentrations decreased (Fig. 5b),

Table 4
Elements that exceeded drinking water quality regulatory limits as set by the USEPA (2011).

Element	Regulatory limit, ppb (MCLG[a]/MCL[b]/SS[c])	Maximum observed aqueous concentration, ppb (Rock)	Comments
As	10 (MCL)	41.3 (Kindblade)	As levels in the Sevy reactor rose to 1057.78 ppb, yet contamination could not be ruled out
Mn	50 (SS)	2827.95 (Cotter)	Mn also exceeded SS and reached 120 ppb in the Sevy reactor
Ni	100 (MCL[d])	891.09 (Sevy)	Ni concentrations in the rest of the beakers were lower than control
Tl	0.5 (MCLG)	1.57 (Cotter)	Tl concentrations in the rest of the beakers were above control, but below MCLG

[a] MCLG: Maximum contaminant level goal (non-enforceable limit, concentrations below which there are no known or expected risk to health).
[b] MCL: Maximum contaminant level (enforceable limit).
[c] SS: Secondary standard (non-enforceable guideline, concentrations above which cosmetic or aesthetic effects in drinking water may occur).
[d] State of California California Code of Regulations, 2011.

presumably due to precipitation of calcium carbonate. Theoretically, calcium carbonate precipitation is contrasted by the calculated undersaturation of calcite (Fig. 6). However, we assumed an atmospheric boundary condition in our calculations of SI values during the decompression stage; in actuality, CO_2 did not immediately and completely degas when the reactors were exposed to the atmosphere, as apparent from the gradual increase in pH (Fig. 5a). When a gradual decrease in pCO_2 was forced on the SI calculations during decompression, the reactors are supersaturated with respect to calcite (not shown).

In contrast to Ca^{2+}, Mg^{2+} concentrations increased during the decompression phase (Fig. 5c), but the causes for this increase are unclear. Mg generally sorbs or precipitates to form carbonate minerals as pH increases, and therefore a decrease in aqueous concentrations was expected. Interestingly, Na^+ concentrations increased during the decompression stage as well.

At the end of the experiments the lids on the beakers were loosened, but not removed, and the beakers depressurized. The pH in the beakers increased immediately after loosening of the lids as CO_2 degassed from the water. This stage of the experiment (Stage F in Fig. 5) does not strictly represent aquifer recovery in a CO_2 leakage scenario because the redox conditions likely changed as oxygen diffused into the beaker and water. However, a corresponding rapid reduction in aqueous metal concentrations was observed with increased pH suggesting possible natural remediation of increased metal concentrations in carbonate aquifers if a CO_2 leak is identified and mitigated. Admittedly, we have no oxygen concentration measurements of the water so we cannot rule out metal oxidation as the cause of the aqueous metal concentration decrease. However, these results highlight the importance of future investigation into geochemical recovery of an aquifer post-leak. These results also suggest that the likelihood of surpassing MCLs in shallow aquifers may, therefore, be highest where CO_2 will not readily degas, such as in a confined USDW, or following long-term (undetected) CO_2 leaks.

5. Conclusions

We conducted a set of dolomite dissolution experiments across a range of pCO_2 conditions, accompanied by thorough characterization of rock and mineral chemistry, in order to understand potential geochemical impacts of CO_2 intrusion into shallow carbonate aquifers. The main conclusions from this work are:

1. Aqueous concentrations of metals increased with increasing pCO_2. Regulatory limits of As, Mn and Ni in drinking water were exceeded in the pressurized experiments, although not for all rocks, and no single rock appeared to be more problematic. Thus, the potential metal contamination is likely to be site specific in dolomitic aquifers.
2. At the end of the experiment, when pCO_2 decreased and pH rebounded, most elements were removed from solution. In context of an actual CO_2 leak into a carbonate aquifer, this result suggests that water quality will be restored to acceptable levels fairly quickly if a point source of CO_2 leakage is detected and remediated.
3. Aqueous concentrations of several trace elements (Sr, Ni, Mn, Tl, Zn) increased due to dissolution of carbonate materials, but the magnitude of the increase was dependent on the specific geochemistry of each rock. Even though oxides and sulfides contained higher mineral-bound concentrations of these trace elements (with the exception of Sr) than carbonates, the dissolution of the carbonate fraction controlled the release of these elements into solution.
4. Calcite dissolution occurs more readily than dolomite dissolution, and inhibits dolomite dissolution to a certain extent, even when calcite is present in minor amounts in a rock that is predominately dolomitic.
5. Published kinetic reaction rates for dolomite, coupled with BET measurements, predicted dolomite dissolution that was much faster than observed in pressurized experiments. A reasonable fit to data was obtained only by assigning a reactive dolomite surface area that was several orders of magnitude lower than the measured BET surface area. This result has been shown by others, but not for reactions related to high partial pressures of CO_2 invading carbonate aquifer materials.

Acknowledgements

This research has been funded by the US Environmental Protection Agency's Science to Achieve Results (STAR) program (Grant RD-83438701-0), but it has not been subjected to any EPA review and therefore does not necessarily reflect the views of the Agency, and no official endorsement should be inferred. In addition, graduate-student fellowship funds to A.W. were donated by Information Handling Services (IHS). J.M. would like to acknowledge support of the LA-ICP-MS work by National Science Foundation Grant CHE-0959226. Cotter Dolomite rock samples were acquired with the generous help of Prof. James Miller from Missouri State University, Springfield, MO. The authors would also like to thank Katie Kirsch, Utpalendu Kuila and Matthew Dye (Colorado School of Mines), and Fred Luiszer, John Drexler and Paul Boni (University of Colorado at Boulder) for help with various analyses and sample preparation.

Appendix A. Supplementary material

Supplementary data associated with this article can be found, in the online version, at http://dx.doi.org/10.1016/j.apgeochem.2013.08.005.

References

Ahmed, I.A.M., Crout, N.M.J., Young, S.D., 2008. Kinetics of Cd sorption, desorption and fixation by calcite: a long-term radiotracer study. Geochim. Cosmochim. Acta 72, 1498–1512.

Alexandratos, V.G., Elzinga, E.J., Reeder, R.J., 2007. Arsenate uptake by calcite: macroscopic and spectroscopic characterization of adsorption and incorporation mechanisms. Geochim. Cosmochim. Acta 71, 4172–4187.

Apps, J.A., Zheng, L., Zhang, Y., Xu, T., Birkholzer, J.T., 2010. Evaluation of potential changes in groundwater quality in response to CO_2 leakage from deep geologic storage. Transp. Porous Media 82, 215–246.

Atchley, A.L., Maxwell, R.M., Navarre-Sitchler, A.K., 2013. Using streamlines to simulate transport in CO_2-impacted drinking water aquifers. Adv. Water Resour. 52, 93–106.

Aurelio, G., Fernandez-Martinez, A., Cuello, G.J., Roman-Ross, G., Alliot, I., Charlet, L., 2010. Structural study of selenium(IV) substitutions in calcite. Chem. Geol. 270, 249–256.

Bardelli, F., Benvenuti, M., Costagliola, P., Di Benedetto, F., Lattanzi, P., Meneghini, C., Romanelli, M., Valenzano, L., 2011. Arsenic uptake by natural calcite: an XAS study. Geochim. Cosmochim. Acta 75, 3011–3023.

Barker, S., Greaves, M., Elderfield, H., 2003. A study of cleaning procedures used for foraminiferal Mg/Ca paleothermometry. Geochem. Geophys. Geosyst. 4 (9), 8407.

Bauer, M., Gassen, N., Stanjek, H., Peiffer, S., 2011. Carbonation of lignite fly ash at ambient T and P in a semi-dry reaction system for CO_2 sequestration. Appl. Geochem. 26, 1502–1512.

Bowen, H.J.M., 1956. Strontium and barium in sea water and marine organisms. J. Mar. Biolog. Assoc. UK 35, 451–460.

Brindley, G.W., Brown, G., 1980. Crystal Structures of Clay Minerals and their X-ray Identification. Monograph 5, Mineralogical Society, London.

Busenberg, E., Plummer, L.N., 1982. The kinetics of dissolution of dolomite in CO_2–H_2O systems at 1.5 °C to 65 °C and O-atm to 1-atm pCO_2. Am. J. Sci. 282, 45–78.

California Code of Regulations, 2011. Maximum Contaminant Levels – Inorganic Chemicals. California Code of Regulations, Title 22, Division 4, Chapter 15, Article 4, § 66431.

Carroll, S., Hao, Y., Aines, R., 2009. Geochemical detection of carbon dioxide in dilute aquifers. Geochem. Trans. 10, 4.
Comans, R.N.J., Middelburg, J.J., 1987. Sorption of trace-metals on calcite - applicability of the surface precipitation model. Geochim. Cosmochim. Acta 51, 2587–2591.
Farrell, R.F., Matthes, S.A., Mackie, A.J., United, S., 1980. A simple, low-cost method for the dissolution of metal and mineral samples in plastic pressure vessels. U.S. Dept. of the Interior, Bureau of Mines, [Washington, D.C.].
Cubillas, P., Köhler, S., Prieto, M., Causserand, C., Oelkers, E.H., 2005. How do mineral coatings affect dissolution rates? An experimental study of coupled $CaCO_3$ dissolution-$CdCO_3$ precipitation. Geochim. Cosmochim. Acta 69, 5459–5476.
Frye, E., Bao, C., Li, L., Blumsack, S., 2012. Environmental controls of cadmium desorption during CO_2 leakage. Environ. Sci. Technol. 46, 4388–4395.
Gautier, J.-M., Oelkers, E.H., Schott, J., 2001. Are quartz dissolution rates proportional to B.E.T. surface areas? Geochim. Cosmochim. Acta 65, 1059–1070.
Harstad, A.O., Stipp, S.L.S., 2007. Calcite dissolution: effects of trace cations naturally present in Iceland spar calcites. Geochim. Cosmochim. Acta 71, 56–70.
Harvey, O.R., Qafoku, N.P., Cantrell, K.J., Lee, G., Amonette, J.E., Brown, C.F., 2013. Geochemical implications of gas leakage associated with geologic CO_2 storage – a qualitative review. Environ. Sci. Technol. 47, 23–36.
Haug, T.A., Kleiv, R.A., Munz, I.A., 2010. Investigating dissolution of mechanically activated olivine for carbonation purposes. Appl. Geochem. 25, 1547–1563.
Hill, M.C., 1998. Methods and Guidelines for Effective Model Calibration. U.S. Geological Survey Water-Resources Investigations, Report 98-4005.
IPCC, 2007. Contribution of working group I to the Fourth Assessment Report of the International Panel on Climate Change. In: Solomon, S.D., Qin, D., Manning, M., Chen, Z., Marquis, M., Averyt, K.B., Tignor, M., Miller, H.L. (Eds.), IPCC Fourth Assessment Report (AR4), Cambridge, UK and New York, NY, USA, pp. 996.
Jackson, M.L., Whittig, L.D., Penningron, R.P., 1950. Segragation procedure for mineralogical analysis of soils. Proc. Soil Sci. Soc. Am. 14, 77–81.
Jochum, K.P., Weis, U., Stoll, B., Kuzmin, D., Yang, Q., Raczek, I., Jacob, D.E., Stracke, A., Birbaum, K., Frick, D.A., Günther, D., Enzweiler, J., 2011. Determination of reference values for NIST SRM 610-617 glasses following ISO guidelines. Geostand. Geoanal. Res. 35, 397–429.
Kamber, B.S., Webb, G.E., 2007. Transition metal abundances in microbial carbonate: a pilot study based on in situ LA-ICP-MS analysis. Geobiology 5 (4), 375–389.
Kharaka, Y.K., Thordsen, J.J., Kakouros, E., Ambats, G., Herkelrath, W.N., Beers, S.R., Birkholzer, J.T., Apps, J.A., Spycher, N.F., Zheng, L., Trautz, R.C., Rauch, H.W., Gullickson, K.S., 2009. Changes in the chemistry of shallow groundwater related to the 2008 injection of CO_2 at the ZERT field site, Bozeman, Montana. Environ. Earth Sci. 60, 273–284.
Kirsch, K., Navarre-Sitchler, A.K., Wunsch, A., McCray, J.E., submitted for publication. CO_2-induced metal release from sandstones: implications for geologic carbon sequestration. Environ. Sci. Technol.
Kulp, J.L., Turekian, K., Boyd, D.W., 1952. Strontium content of limestones and fossils. Bull. Geol. Soc. Am. 63, 701–716.
Li, X.D., Coles, B.J., Ramsey, M.H., Thornton, I., 1995. Sequential extraction of soils for multielement analysis by ICP-AES. Chem. Geol. 124, 109–123.
Little, M.G., Jackson, R.B., 2010. Potential impacts of leakage from deep CO_2 geosequestration on overlying freshwater aquifers. Environ. Sci. Technol. 44, 9225–9232.
Lu, J.M., Partin, J.W., Hovorka, S.D., Wong, C., 2010. Potential risks to freshwater resources as a result of leakage from CO_2 geological storage: a batch-reaction experiment. Environ. Earth Sci. 60, 335–348.
MacInnis, I.N., Brantley, S.L., 1992. The role of dislocations and surface morphology in calcite dissolution. Geochim. Cosmochim. Acta 56, 1113–1126.
Moore, D.M., Reynolds, R.C., 1997. X-ray Diffraction and the Identification and Analysis of Clay Minerals. Oxford University Press, Oxford, UK.
Navarre-Sitchler, A.K., Maxwell, R.M., Siirila, E.R., Hammond, G.E., Lichtner, P.C., 2013. Elucidating geochemical response of shallow heterogeneous aquifers to CO_2 leakage using high-performance computing: implications for monitoring of CO_2 sequestration. Adv. Water Resour. 53, 45–55.
Orlando, A., Lelli, M., Marini, L., 2012. Production of amorphous hydrated impure magnesium carbonate through ex situ carbonation. Appl. Geochem. 27, 2500–2510.
Palandri, J.L., Kharaka, Y.K., 2004. A Compilation of Rate Parameters of Water–Mineral Interaction Kinetics for Application to Geochemical Modeling. US Geological Survey Open File Report 2004-1068. US Geological Survey Open File Report 2004-1068, pp. 64.
Parkhurst, D.L., Appelo, C.A.J., 1999. User's Guide to PHREEQC (version 2): A Computer Program for Speciation, Batch Reaction, One-Dimensional Transport, and Inverse Geochemical Calculations. U.S. Geological Survey Water Resources Investigations 99-4259.
Perez-Lopez, R., Montes-Hernandez, G., Nieto, J.M., Renard, F., Charlet, L., 2008. Carbonation of alkaline paper mill waste to reduce CO_2 greenhouse gas emissions into the atmosphere. Appl. Geochem. 23, 2292–2300.
Pingitore, N.E., Lytle, F.W., Davies, B.M., Eastman, M.P., Eller, P.G., Larson, E.M., 1992. Mode of incorporation of Sr^{2+} in calcite – determination by X-ray absorption-spectroscopy. Geochim. Cosmochim. Acta 56, 1531–1538.
Poeter, E.P., Hill, M.C., Banta, E.R., Mehl, S., Christensen, S., 2005. UCODE_2005 and Six Other Computer Codes for Universal Sensitivity Analysis, Calibration, and Uncertainty Evaluation. U.S. Geological Survey Techniques and, Methods 6-A11, pp. 283.
Pokrovsky, O.S., Golubev, S.V., Schott, J., 2005. Dissolution kinetics of calcite, dolomite and magnesite at 25 °C and 0 to 50 atm pCO_2. Chem. Geol. 217, 239–255.
Pokrovsky, O.S., Golubev, S.V., Schott, J., Castillo, A., 2009. Calcite, dolomite and magnesite dissolution kinetics in aqueous solutions at acid to circumneutral pH, 25 to 150 degrees C and 1 to 55 atm pCO_2: new constraints on CO_2 sequestration in sedimentary basins. Chem. Geol. 265, 20–32.
Pokrovsky, O.S., Schott, J., 2001. Kinetics and mechanism of dolomite dissolution in neutral to alkaline solutions revisited. Am. J. Sci. 301, 597–626.
Prissok, F., Lehmann, G., 1986. An electron-paramagnetic-res study of Mn^{2+} and Fe^{3+} in dolomites. Phys. Chem. Miner. 13, 331–336.
Querol, X. et al., 2001. Determination of element affinities by density fractionation of bulk coal samples. Fuel 80 (1), 83–96.
Radu, T., Subacz, J.L., Phillippi, J.M., Barnett, M.O., 2005. Effects of dissolved carbonate on arsenic adsorption and mobility. Environ. Sci. Technol. 39 (20), 7875–7882.
Reeder, R.J., Lamble, G.M., Lee, J.F., Staudt, W.J., 1994. Mechanism of SeO_4^{2-} substitution in calcite – an XAFS study. Geochim. Cosmochim. Acta 58, 5639–5646.
Reeder, R.J., Lamble, G.M., Northrup, P.A., 1999. XAFS study of the coordination and local relaxation around Co^{2+}, Zn^{2+}, Pb^{2+}, and Ba^{2+} trace elements. Am. Mineral. 84, 1049–1060.
Saldi, G.D., Jordan, G., Schott, J., Oelkers, E.H., 2009. Magnesite growth rates as a function of temperature and saturation state. Geochim. Cosmochim. Acta 73, 5646–5657.
Siirila, E.R., Navarre-Sitchler, A.K., Maxwell, R.M., McCray, J.E., 2012. A quantitative methodology to assess the risks to human health from CO_2 leakage into groundwater. Adv. Water Resour. 36, 146–164.
Skold, M.E., Thyne, G.D., McCray, J.E., 2007. Using UCODE_2005 and PHREEQC to determine thermodynamic constants from experimental data. Ground Water 45, 368–373.
Sø, H.U., Postma, D., Jakobsen, R., Larsen, F., 2008. Sorption and desorption of arsenate and arsenite on calcite. Geochim. Cosmochim. Acta 72, 5871–5884.
Staudt, W.J., Reeder, R.J., Schoonen, M.A.A., 1994. Surface structural controls on compositional zoning of SO_4^{2-} and SeO_4^{2-} in synthetic calcite single-crystals. Geochim. Cosmochim. Acta 58, 2087–2098.
Sturchio, N.C., Antonio, M.R., Soderholm, L., Sutton, S.R., Brannon, J.C., 1998. Tetravalent uranium in calcite. Science 281, 971.
Tang, Y.Z., Elzinga, E.J., Lee, Y.J., Reeder, R.J., 2007. Coprecipitation of chromate with calcite: batch experiments and X-ray absorption spectroscopy. Geochim. Cosmochim. Acta 71, 1480–1493.
Trautz, R., Pugh, J., Varadharajan, C., Zheng, L., Bianchi, M., Nico, P.S., Spycher, N., Newell, D.L., Esposito, R.A., Wu, Y., 2013. Effect of dissolved CO_2 on a shallow groundwater system: a controlled release field experiment. Environ. Sci. Technol. 47, 298–305.
USEPA, 2011. 2011 Edition of the Drinking Water Standards and Health Advisories. Office of Water, U.S. Environmental Protection Agency, Washington, DC. EPA 820-R-11-002.
Wang, S., Jaffe, P.R., 2004. Dissolution of a mineral phase in potable aquifers due to CO2 releases from deep formations; effect of dissolution kinetics. Energ. Convers. Manage. 45, 2833–2848.
Washton, N.M., Brantley, S.L., Mueller, K.T., 2008. Probing the molecular-level control of aluminosilicate dissolution: a sensitive solid-state NMR proxy for reactive surface area. Geochim. Cosmochim. Acta 72, 5949–5961.
Wei, Y., Maroto-Valer, M., Steven, M.D., 2011. Environmental consequences of potential leaks of CO_2 in soil. Energy Proc. 4, 3224–3230.
White, A.F., Peterson, M.L., 1990. Role of reactive surface area characterization in geochemical models. In: Melchior, D.C., Bassett, R.L. (Eds.), Chemical Modelling of Aqueous Systems II. pp. 461–475.
Wilkin, R.T., DiGiulio, D.C., 2010. Geochemical impacts to groundwater from geologic carbon sequestration: controls on pH and inorganic carbon concentrations from reaction path and kinetic modeling. Environ. Sci. Technol. 44, 4821–4827.
Wright, K., Cygan, R.T., Slater, B., 2002. Impurities and nonstoichiometry in the bulk and on the (1014) surface of dolomite. Geochim. Cosmochim. Acta 66, 2541–2546.
Wunsch, A., Navarre-Sitchler, A.K., Moore, J., McCray, J.E., submitted for publication. Metal release from limestones at high partial-pressures of CO_2. Chem. Geol.
Yokoyama, Y., Tanaka, K., Takahashi, Y., 2012. Differences in the immobilization of arsenite and arsenate by calcite. Geochim. Cosmochim. Acta 91, 202–219.
Zheng, L., Apps, J.A., Spycher, N., Birkholzer, J.T., Kharaka, Y.K., Thordsen, J., Beers, S.R., Herkelrath, W.N., Kakouros, E., Trautz, R.C., 2012. Geochemical modeling of changes in shallow groundwater chemistry observed during the MSU-ZERT CO_2 injection experiment. Int. J. Greenhouse Gas Control 7, 202–217.